Institute of Pharmaceutical Chemistry[1], Department of Pharmacy, Institute of Applied Dermatopharmacy[2], Institute of Physical Chemistry[3], Department of Chemistry, Martin-Luther-Universität Halle-Wittenberg, Germany

Characterization of dimethyldiacyloxysilanes by differential scanning calorimetry, Raman scattering and X-ray diffraction

P. Pallas[1], S. Wartewig[2], I. Zimmermann[3] and H. Richter[1]

The phase behaviour of diacyloxydimethylsilanes (DMS Cn; n = 10, 12, 14, 16, 18, 20, 22) was investigated by differential scanning calorimetry, X-ray diffraction and Raman spectroscopy. All DMS Cn melt from a crystalline phase to an isotropic liquid with a single sharp transition. On cooling, the homologoues DMS C16 up to DMS C22 show a characteristic monotropic phase ($L\beta'_H$). In contrast to the calorimetrical investigations, it was not possible to analyse the monotropic phase of DMS C16 by X-ray diffraction. This behaviour is due to a two-phase region (gel phase – crystalline phase). The Raman spectra of all DMS are very similar. Only in the low frequency range we find different bands of the longitudinal acoustic modes. The Raman measurements demonstrate undoubtedly that in the solid state the alkyl chains are in all-*trans* conformation. The factor group splitting of the CH_2 scissoring Raman mode show that the DMS Cn are arranged in a subcell packing with two molecules per unit cell. The highly ordered all-*trans* structure of the alkyl chains is present up to the melting transition. On melting there are changes in different regions of the Raman spectra: C–H stretching, CH_2 scissoring mode, C–C skeletal stretching, CH_3 rocking and longitudinal acoustic modes. On cooling DMS C18 and DMS C20 from the melt to the crystalline state, the gel phase is also proved by Raman scattering. Based on the results of the Raman and X-ray data the gel phase is characterized by a hexagonal subcell packing and by an ordered structure of the alkyl chain residues.

1. Introduction

Siosomes® as a new class of vesicles are a recent invention [1–5]. They are prepared from organo-silicon-compounds and consist for instance of long chains of di(acyloxy)dimethylsilanes. These organo-silicon-compounds proved to be amphiphilic and were found to be Siosome® formers [2]. The hydrophilic zone is formed by the free oxygen electron pairs of the ester structure while the two long hydrocarbon chains (number of the carbon atoms are 10, 12, 14, 16, 18, 20) are the lipophilic part. The names of the structures are: DMS C10 for di(decanoyloxy)dimethylsilane or DMS C12 for di(dodecanoyloxy)dimethylsilane, and so on.

Similar to liposomes, Siosomes® can accumulate water-soluble substances in their vesicular interior and lipophilic substances in the lipophilic area formed by the hydrocarbon chains of the fatty acid derivatives [4]. For understanding the formation of vesicles from these substances, it is essential to know at first the structural properties at the pure substances.

In order to describe the physico-chemical properties of the designated diacyloxydimethylsilanes and to analyse their phase behaviour, we have used differential scanning calorimetry, Raman spectroscopy and X-ray diffraction [6, 7]. All these methods describe, independently of each other, the phase behaviour of diacyloxydimethylsilanes. Diacyloxydimethylsilanes DMS Cn with acyloxy-chains of varying length (n = 10, 12, 14, 16, 18 and 20 carbon atoms) were investigated in order to evaluate the lipophilic influence on the phase behaviour.

2. Investigations, results and discussion

2.1. Differential Scanning Calorimetry

The thermotropic behaviour of DMS C10...20 has been reported in a recent publication [3]. Fig. 1 shows, for example, the DSC curves of DMS C16.

All DMS Cn exhibit a high enthalpic transition from the crystalline state to an isotropic liquid (about 40 kJ/mol for DMS C 10 and 150 kJ/mol for DMS C 20)[3]. The substance DMS C18 shows, on cooling, a characteristic monotropic phase designated as $L_{\beta'H}$. This phase manifests itself and is temporary stable especially for substances with a chainlength from C18 upwards. In the case of DMS C16, the monotropic phase disappears immediately and even tempering did not provide a sufficient stabilization.

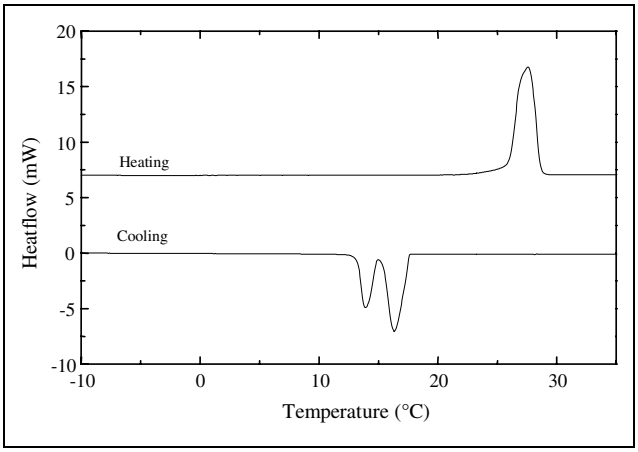

Fig. 1: DSC thermogram of DMS C16

Despite tempering, the monotropic phase could not be stabilised sufficiently. Based on the results of the DSC investigations, a further characterization of the phases was carried out by X-ray diffraction and Raman spectroscopy.

2.2. X-ray-diffraction

Figures 2 to 5 show the scattering curves of dried DMS C16 and DMS C18 on heating and cooling, respectively.

The reciprocal long spacings in the scattering curve of DMS C16 at −30 °C show a ratio of $s_1 : s_2 : s_3 = 1 : 2 : 3$ indicating that the molecules are arranged in a lamellar structure with a layer distance of $d_L = 2.43$ nm ($s = 0.411$ nm^{-1}). A number of sharp wide-angle peaks

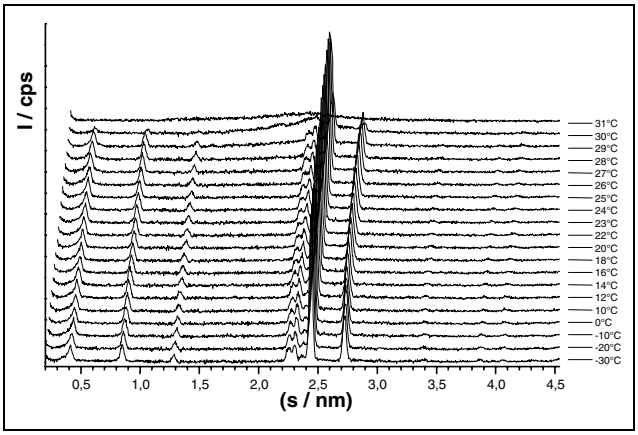

Fig. 2: Scattering curve of DMS C16 (heating)

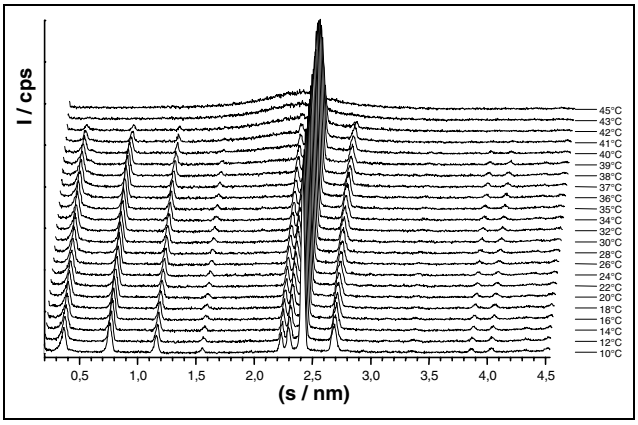

Fig. 3: Scattering curve of DMS C18 (heating)

characterize the phase at $-30\,^{\circ}C$ as a crystalline phase. The dominant chain reflections are localized at $s = 2.442$ and 2.727 nm. Only at 30 °C a change in the peak intensities was observed which is due to the melting of the substance. The sharp short spacings transform into a diffuse scattering caused by fluid chains. The lack of long spacings in the phase above 31 °C is a strong evidence for the isotropic state.

On cooling to 24 °C, the typical short spacings of the crystalline phase reappear with a weak intensity (Fig. 4). At 23 °C the layer structure is reconstructed and a repeat distance of $d_L = 2.43$ nm is observed. In the case of DMS C 16, it was not possible to analyze the monotropic phase because the substance recrystallizes during the recording time of 60 s.

The scattering behaviour of DMS C18 also indicates a lamellar crystalline phase with an increased d_L-value (2.73 nm). The identical peak positions of DMS C16 and DMS C18 in the wide-angle part demonstrate the same crystalline phase.

With respect to the repeat distance of the crystalline phase of DMS C16, we observed an increase of 0.30 nm. Using the dependence of the d_L-value on the chain length, it is possible to calculate the chain tilt angle with respect to bilayer norms. It is well-known [8] that the bilayer distance increases by 0.254 nm per CH_2-group for chains arranged perpendicular to the bilayer plane. From this dependence a chain tilting of 54° can be estimated.

The melting of the substance begins at 40 °C with a decrease in the scattered intensity. At 43 °C the substance is isotropic.

Cooling the sample, the scattering curve at 34 °C shows only one sharp short spacing at $s = 2.420\ nm^{-1}$, whose

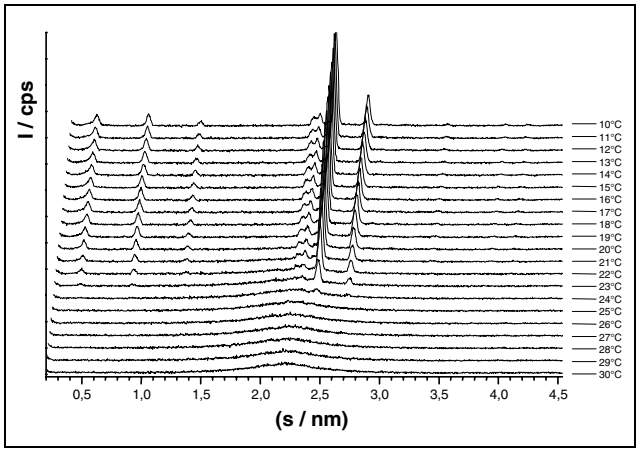

Fig. 4: Scattering curve of DMS C16 (cooling)

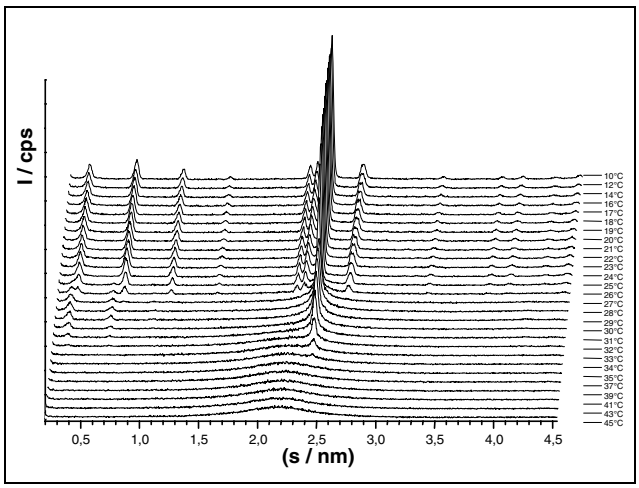

Fig. 5: Scattering curve of DMS C18 (cooling)

intensity increases on further cooling. Such a pattern is usually interpreted as a scattering of a 2D hexagonal subcell [9]. The integral half band width of $B_{1/2} = 0{,}180\ nm^{-1}$ for this chain scattering indicates the tilting of the chains [10]. From the short spacing, a hexagonal lattice constant of 0.477 nm can be calculated. From the cross-section per chain of 0.197 nm^2 a gel phase can be derived [9]. At 31 °C a bilayer distance of $d_L = 3.17$ nm in its second order was found.

In the scattering curve at 26 °C, among the long spacings of the gel phase a new long spacing with its second order occurs at $d = 2.73$ nm; its intensity increases with simultaneous disappearance of the long spacings of the gel phase. This behaviour is due to a two-phase region (gel phase – crystalline phase).

The substance recrystallizes finally at 24 °C.

2.3. Raman Spectroscopy

The Raman spectra of all DMS substances are very similar. The major part of the spectra consists of bands ascribed to the alkyl chain residue, but there are also bands of lower intensity, that belong to the head group of the lipid. The band assignments for DMS C20 according to literature data [11] are summarized in Table 1.

The band positions for the other substances investigated are the same except for the bands in the low frequency range. In the low frequency range we find the bands of the longitudinal acoustic modes (LAM 3, see Table 2) for all samples in the crystalline state. The peak positions of

Table 1: Observed FT-Raman bands for DMS C20 at −30 °C and assignments according to literature data [7, 11] (band position in cm^{-1}, accuracy <1 cm^{-1})

Band position	Assignment
100 s	LAM-3
292 w	LAM-5
378 w	δ (CCC) skeletal backbone
868 mw	CH_3 rocking, Si−CH_3
892 mw	CH_3 rocking, chain end tt
1062 m	ν_{as} (C−C), alkyl chain with trans units
1111 mw	ν (Si−O−C)
1131 m	ν_s (C−C), alkyl chain with trans units
1173 w	CH_2 rocking
1295 s	CH_2 twisting
1371 w	CH_2 wagging
1417 m 1442 s 1465 m	CH_2 scissoring, splitting due to Fermi resonance with CH_2 rocking, factor group splitting
1738 mw	ν(C=O)
2723 mw	overtones/combinations of δ (CH_2)
2847 vs	ν_s (CH_2)
2881 vs	ν_{as} (CH_2)
2899 s, br, sh 2932 s, br	Fermi resonance of ν_s (CH_2) and overtones of CH_2 scissoring, ν_s (CH_3)
2957 m	ν_{as} (CH_3)

v very; s strong; m medium; w weak; br broad; sh shoulder; δ deformation; ν_{as} asymmetric stretching; ν_s symmetric stretching

the LAM obey the rule: the longer the alkyl chain length, the lower the wavenumber (Fig. 6). This finding undoubtely demonstrates for all solid DMS Cn that the alkyl chains are in the all-*trans* (planar zig-zag) conformation. The appearance of the symmetric and asymmetric C−C stretchings bands and of the asymmetric CH_2 stretching band, characteristic of three or more trans bonds in sequence [12], confirms this highly ordered structure of chains. Furthermore, the sharp methyl rocking mode at 891 cm^{-1} shows that the chain ends are also in the tt-conformation [13].

The factor group splitting of the CH_2 scissoring vibrations observed for all samples in the solid state indicates that the subcell of DMS Cn comprises two molecules.

By increasing the temperature, we observed changes in different regions of the Raman spectra. Fig. 7 illustrates the temperature dependency of the C−H stretching vibrations (2800–3000 cm^{-1}), of the CH_2 scissoring mode (1400–1480 cm^{-1}), of the C-C skeletal stretching vibrations (1000–1150 cm^{-1}), and of the CH_3 rocking vibrations (830–900 cm^{-1}) for the DMS C20 sample.

The striking feature on increasing temperature is that the intensity of the asymmetric CH_2 stretching band, at about 2880 cm^{-1}, decreases and disappears in the underlying background above the melting point. In order to quantify this effect, the overlapping bands were decomposed using the OPUS fit procedure. Fig. 8 shows as an example the result of the composition for DMS C20. The temperature dependence of the integrated intensity of the symmetric and asymmetric CH_2 stretching bands was determined accordingly. As shown in Fig. 9, the normalized intensity ratio $I[\nu_{as}(CH_2)]/I[\nu_s(CH_2)]$, as a yardstick of the relative population of the *trans* and *gauche* conformers of the alkyl chains, starts decreasing substantially near 36 °C and tends to zero at the melting point. The transition range amounts to $\Delta T \sim 5$ K. The same behaviour was found for all other samples, but, with the variation that the transition range becomes smaller for samples with shorter chain residues, e.g. $\Delta T \sim 2$ K for DMS C10.

Table 2: Band position of LAM-3 for DMS C10 to C20 at −30 °C

	C20	C18	C16	C14	C12	C10
ν(cm^{-1})	100	108	120	134	152	179

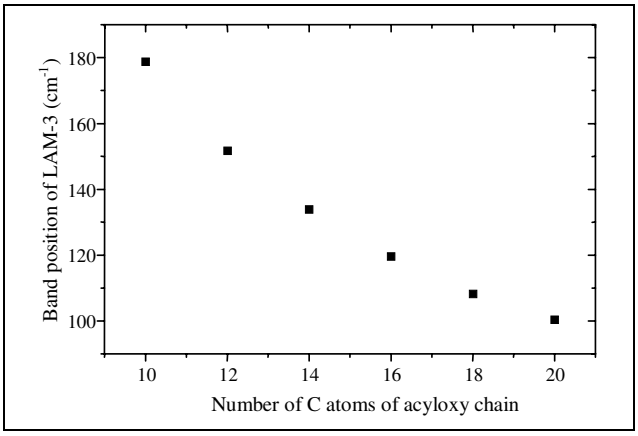

Fig. 6: Chain length dependence of LAM 3

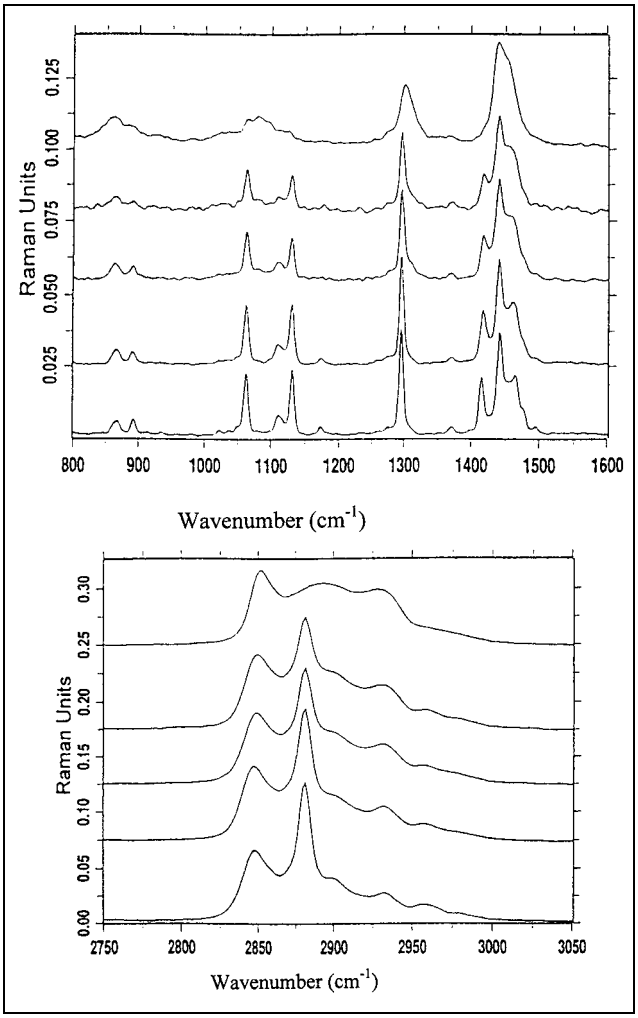

Fig. 7: Temperature dependence of the Raman spectra of DMS C20 in the spectral range. (a) 800–1600 cm^{-1} and (b) 2750–3050 cm^{-1}. Temperature from top to bottom. 41,1 °C, 39,7 °C, 39,0 °C, 24,5 °C and −30,0 °C

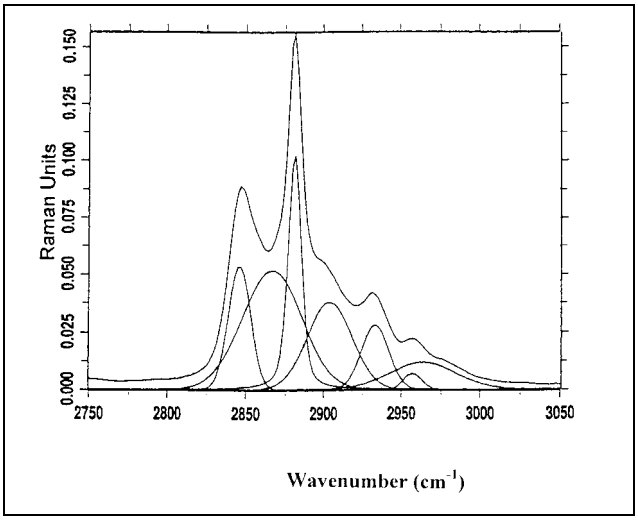

Fig. 8: Decomposition of the CH_2 stretching band

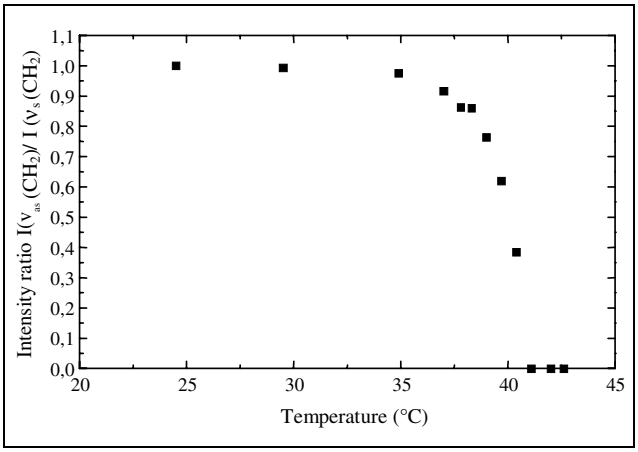

Fig. 9: Temperature dependence of the normalized intensity ratios I [$\nu_{as}(CH_2)$]/I [$\nu_s(CH_2)$] for DMS C20

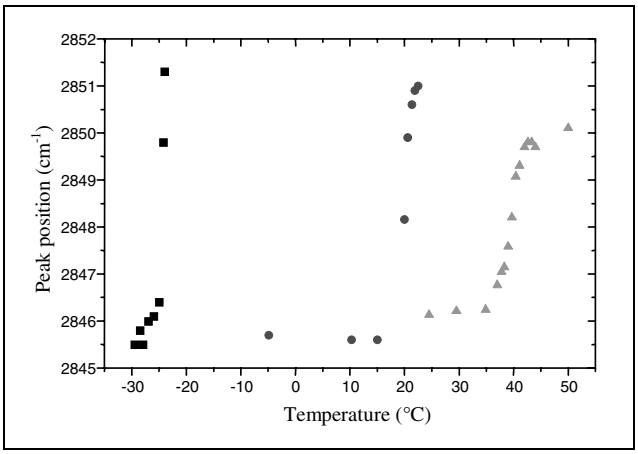

Fig. 10: Temperature dependence (heating) of the peak position of $\nu_s(CH_2)$ for (□) DMS C10, (○) DMS C16 and (▽) DMS C20

Furthermore, it appears that the band position of $\nu_s(CH_2)$ is very sensitive for monitoring the *trans/gauche* transformation within the hydrocarbon chain. The temperature dependence of the peak position of this band for DMS C20, DMS C16 and DMS C10 is displayed in Fig. 10. These curves indicate once again that the transition range for DMS C10 is smaller than that for DMS C20.

The factor group splitting of the CH_2 scissoring vibration vanishes in the course of melting in all samples. Fig. 11

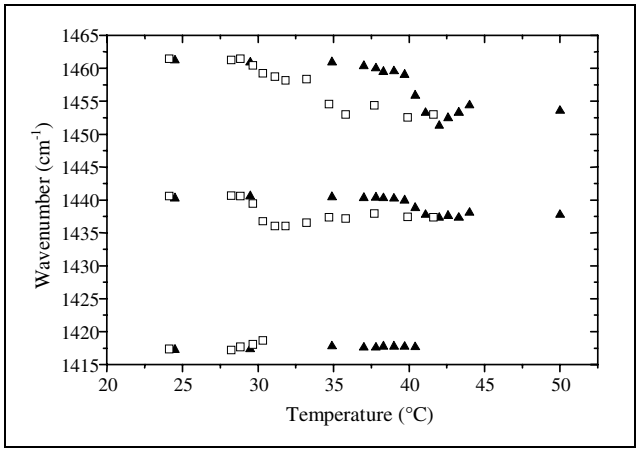

Fig. 11: Temperature dependence of the factor group splitting of DMS C20. (▽) Heating and (□) Cooling

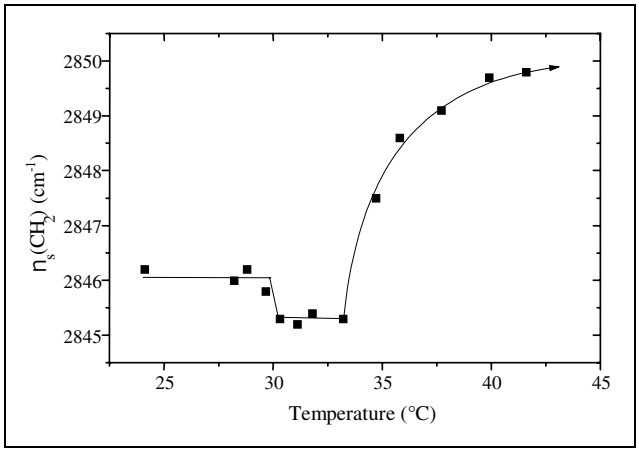

Fig. 12: Temperature dependence (cooling) of $\nu_s(CH_2)$ for DMS C20

shows the temperature dependence of this splitting in the case of DMS C20.

Another point of interest is that for all samples, the symmetric and asymmetric C−C stretching modes, which belong to *trans* conformers (3 or more *trans* bonds in sequence), disappear on melting in the same way as the asymmetric CH_2 stretching band. On the other hand, the intensity of the C-C stretching mode, owing to hydrocarbon chains with gauche units, increases continuously. The intensity of the LAM band decreases with increasing temperature owing to the fact that the number of alkyl chain residues in all-*trans* conformation decreases. However, their wavenumbers are almost temperature independent, which indicates that all-*trans* chains exist up to melting point. In the melt, the broad disorder-LAM band appears at about 215 cm^{-1} for all samples.

In summary, the spectroscopic data demonstrate that DMS Cn are arranged in a subcell packing with two molecules per unit cell. The highly ordered all-*trans* structure of the alkyl chains is present up to the melting transition.

Cooling the samples DMS C20 and DMS C18 from the melt to the crystalline state, the gel phase $L\beta'_H$ appears, which is also documented by Raman data. This behaviour is very pronouced for DMS C20 where bands belonging to *trans* sequences of the alkyl chains become visible at a temperature of about 36 °C. Fig. 12 illustrates this for the band position of the symmetric stretching CH_2 band. The LAM 3 band can likewise be identified at 36 °C. On the other hand, the factor group splitting of the CH_2 scissoring mode occurs for the first time at about 30 °C

(see Fig. 11). The band position of LAM 3 is the same in both phases. However, the bandwidth is different, namely 15.5 cm^{-1} for the intermediate phase and 10.5 cm^{-1} for the crystalline phase. Based on these results it can be assumed that the intermediate phase is characterized by a hexagonal subcell packing and by an ordered structure of the alkyl chain residues. In the case of DMS C18, the intermediate phase covers only the small temperature interval of 1 °C.

In conclusion, DSC, X-ray and Raman spectroscopy are suitable analytical methods to describe the physico-chemical properties of dried solid diacyloxydimethylsilanes. A highly ordered all-*trans* chain conformation was found for all DMS Cn in the crystalline state, which is present up to the melting transition. The experimental findings indicate that the chains are arranged in a subcell packing with two molecules per unit cell, where the chain tilt angle is 54°. It is to notice that the substances DMS Cn with $n > 16$ exhibit a characteristic monotropic phase ($L\beta'_H$) on cooling. Based on X-ray and Raman data it can be assumed that this intermediate phase is characterized by a hexagonal subcell packing and tilted chains.

3. Experimental

3.1. Sample preparation

All dimethylacyloxysilanes were characterized by ^{1}H-, ^{13}C- and ^{29}Si-NMR [1]. The polycristalline silanes were chromatographically pure. All compounds were investigated in a solid form.

3.2. Differential scanning calorimetry

The calorimetrical measurements were performed with a DSC-2 Perkin-Elmer differential scanning calorimeter. The mass size was about 2 mg and the scanning rate used 5 $K \cdot min^{-1}$. The transition temperature was determined as onset temperature by extrapolation of the most rapid rise in the excess heat capacity curve as a function of temperature. The enthalpy change was determined from the area under the transition peak by comparison with that for a known standard (indium, water).

3.3. X-Ray powder diffraction

The X-ray investigation were carried out using the STOE Diffractometer (STOE & CIE, Darmstadt) with an X-ray generator ID 3000 (Seifert FPM, Freiberg).

A curved germanium monochromator (Johann-Typ) mounted on the circumference of the diffractometer supplies a convergent monochromatic $CuK\alpha_1$ X-ray beam ($\lambda = 0.154051$ nm). X-ray diffraction data were recorded using a stationary position sensitive detector. The recording time of one scattering curve at each temperature was 60 s.

The temperature range from −30 °C to 45 °C was controlled within an accurancy of +/−0.1 K. Liquid nitrogen was used as cooling agent. In all cases samples were contained in thin-walled capillary tubes with a diameter of 1.0 nm.

3.4. Fourier transform Raman spectroscopy

The Raman spectra were acquired using a Bruker Fourier transform IR spectrometer IFS 66 equipped with the Raman module FRAU 106. A diode pumped Nd : YAG laser, which emits at a wavelength of 1064 nm, was used as the excitation source. The scattered radiation was collected at 180° to the source. Typical spectra were recorded with a laser power of 200 mW at sample location and a resolution of 4 cm^{-1}.

In order to improve the signal to noise ratio 400 scans were coadded, corresponding to a measurement time of 10 min. The recorded frequencies are reproducible to within 1 cm^{-1}. Using the temperature accessory R 495, the temperature dependency of the Raman spectra was studied. After a temperature step, the sample was allowed to equilibrate for 15 min to stabilize the temperature before recording each spectrum. The manipulation and evaluation of the spectra, in particular, the integration and curve fitting were carried out using the Bruker OPUS software. Generally, Raman intensities were determined as integrated band intensities.

Aknowledgement: This work was supported by the Deutsche Forschungsgemeinschaft, Sonderforschungsbereich 197.

References

1 Richter, H.; Kunath, U.; Salama, Z. B.; Nuhn, P.; Nindel, H.: Pharmazie **47**, 300 (1992)
2 Richter, H.; Salama, Z. B.; Kunath, U.; Meyer, H. W.; Nindel, H.; Nuhn P.: Pharmazie **47**, 385 (1992)
3 Pallas, P.; Richter H.: Pharmazie **50**, 634 (1995)
4 Salama, Z. B.; Richter, H.; Kunath, U.; Strube, M.; Nuhn, P.; Meyer, H.W; Nindel, H.: APC 07F/343 281-0, EP 0483 465 A1
5 Salama, Z. B.; Jaeger, H.: Biotech. Forum Europe, **9**, 235 (1992)
6 Verma, S. P.; Wallach, D. F. H.: in D. Chapman (Ed.), Biomembrane structure and function S. 167, Verlag Chemie, Weinheim, 1984
7 Cao, A.; Liquier, J.; Tailandier, E.: in Schrader, B. (Ed.) IR and Raman spectroscopy S. 344, Verlag Chemie, Weinheim, 1995
8 Small, M. D.: Handbook of Lipid Res. 4. New York, London, Plenum Press
9 Tardieu, A.; Luzatti, V.; Reman, F. C.: J. Mol. Biol. **75**, 711 (1973)
10 Furuya K.; Mitsui T.: J. Phys. Soc. Jap. **46**, 611 (1979)
11 Dollish, F. R.; Fateley, W. G.; Bentley F. F.: Characteristic Raman frequencies of organic compounds Wiley and sons, New York (1973)
12 Brown, K. G.; Bicknell-Brown, E.; Ladjadj, M.: J. Chem. Phys. **91**, 3436 (1987)
13 Hendra, H. P.; Jobic, E. P.; Marden, E. P.; Bloor, D.: Spectrochem. Acta **33A**, 445 (1977)

Received August 30, 1999
Accepted November 15, 1999

Prof. Dr. H. Richter
FB Pharmazie der
Martin-Luther-Universität
Wolfgang-Langenbeck-Str. 4
D-06120 Halle